TITLE PAGE

Title: Population temporal structure supplements the rate code during sensorimotor transformations

Abbreviated title: Population temporal dynamics in gaze control

Authors: Uday K. Jagadisan[1,3] and Neeraj J. Gandhi[1,2,3]

Author affiliations:
[1]Department of Bioengineering
[2]Department of Neuroscience
[3]Center for the Neural Basis of Cognition
University of Pittsburgh, Pittsburgh, PA 15213

Corresponding author: Uday K. Jagadisan
153 Eye and Ear Institute
203 Lothrop St
Pittsburgh, PA 15213
USA
Tel: +1-315-4099934
E-mail: kj.udayakiran@gmail.com

Author Contributions: U.K.J and N.J.G designed the study. U.K.J. performed the experiments, analyzed the data, and performed model simulations. U.K.J and N.J.G wrote the manuscript.

Number of pages: 25

Number of figures: 4 + 6 extended figures

Number of words: Abstract - 345, Main text - 2078, Supplementary text - 669, Methods - 2895

Conflict of interest: The authors declare no competing financial interests.

Acknowledgements: We thank Drs. A. Batista, C. Olson, M. Smith, and B. Yu for scientific discussions and critical feedback on previous versions of the manuscript and J. McFerron for programming assistance. The study was funded by the following NIH R01 grants: EY022854 and EY024831 awarded to N.J.G.

Abstract

In order to successfully interact with the environment the brain must funnel down the sensory inputs it receives to specific movements at specific times. Such sensory-to-motor transformations are critically mediated by neurons in premotor brain networks whose evolving activities represent sensory, cognitive, and movement-related information[1-3]. However, this multiplexing poses a conundrum – how does a decoder know precisely when to initiate a movement if such neurons are also active at times other than when a movement occurs (e.g., in response to sensory stimulation)? Extant models of movement generation that rely on firing rate, including rise-to-threshold[4], inhibitory gating[5], and dynamical switches at the population level[6,7], leave certain explanatory gaps unfilled. Here, we propose a novel hypothesis: movement is triggered not only by an increase in firing rate, but critically by a reliable temporal pattern in the population response. We show that in brain regions involved in orienting eye movements - the superior colliculus (SC) and the frontal eye fields (FEF) - the temporal dynamics between neurons during visually-driven activity is different from that during pre-movement activation. Specifically, using a measure that captures the fidelity of the population code - here called temporal stability - we show that the temporal structure fluctuates in the visual response but remains stable during the pre-movement response, thus distinguishing incoming sensory input from motor output. This is an important attribute because SC and FEF "visuomovement" neurons project directly to the brainstem[8,9] which houses the controller for gaze shifts, and any increase in the incoming drive is poised to trigger a (potentially undesirable) gaze shift. We also demonstrate that a simple firing rate-based network with synaptic facilitation can distinguish between stable and fluctuating population codes, suggesting a putative mechanism for interpreting temporal structure. These findings offer an alternative perspective on the relationship between spatial attention and motor preparation[10,11] by situating the correlates of movement initiation in the temporal features of activity in shared neural substrates. They also suggest a need to look beyond the instantaneous rate code and consider the effects of short-term population history on neuronal communication and its effects on behaviour.

Main text

Across brain regions involved in the control of gaze, including the SC in the midbrain and the FEF in the neocortex, so-called visuomovement neurons burst a volley of spikes both in response to a visual stimulus and for generating a gaze shift or saccade to the spatial location of the stimulus[1]. The dual nature of visuomovement neurons is best illustrated by examining their activity in the delayed response paradigm (Figure 1A). In this task, the subject is required to withhold a saccade in response to the presentation of a stimulus in the visual periphery until after the disappearance of a central fixation cue. Figure 1C shows the average activity aligned on target (left) and saccade (right) onsets for 57 SC and 22 FEF neurons in two monkeys (*Macaca mulatta*). The visual response exhibits a high frequency burst, reaching levels observed 30-40 ms prior to saccade onset, yet the former rise does not trigger a movement while the latter does. In fact, it is not uncommon to find neurons whose peak visual response is greater than peak pre-movement activation[12], an observation that casts doubt on thresholding[4] as a singular mechanism. Given that such neurons project directly to the brainstem saccade burst generator that initiates and guides saccadic gaze shifts[8,9] (Figure 1B), we asked how downstream structures are able to differentiate between the two bursts.

Previous studies have examined the across-trial reliability of neural responses as a correlate of behavioural states[13-15], including movement preparation[16]. We computed the Fano factor, a ratio of the spike count variance to the mean across trials. In both SC and FEF, the Fano factor decreased prior to saccade onset (Figure 1D), but showed a mixed pattern during the visual burst following stimulus onset (decrease in FEF and a transient increase in SC). Thus, spike count reliability alone is insufficient to explain the lack of a saccade during the high-frequency visual burst. More importantly, since reliability is necessarily computed across trials, the brain cannot use this information to make movement decisions on any given trial.

Zooming in on the activity profiles of individual neurons at the time of the visual and premotor bursts (Figure 2A, insets) sheds light on a possible solution to this puzzle. Qualitatively, the neurons' firing profiles seem to be unstructured in the visual burst, while they rise more coherently in the premotor burst. We hypothesized that the degree to which the relative levels of activation across the population is preserved over the course of a burst controls saccade initiation. To quantify this, we created a pseudo-population of our single-unit recordings and constructed a trajectory of population activity over time. We normalized the population vector at each time point, which constrains it to a unit hypersphere in state space. This step factors out global changes in firing across the population and focuses on the relative activity levels. We then computed the dot product between two of these unit vectors separated in time (20 ms here) - we call this the temporal stability of the population code. This procedure is schematized in Figure 2B (for details, see Online Methods and Extended Data Figure 1). Figure 2C shows the evolution of temporal stability of the SC and FEF populations (solid and dotted traces, respectively, inset shows individual animals). In both regions, the population code is relatively unstable during the visual burst and remains stable during the premotor burst. This was true across a range of separation times between the population vectors (EDF 2). Thus, the stability across the population of visuomovement neurons seems to function as a switch that prevents movement initiation at an undesirable time (visual epoch), allowing the animal to successfully perform the task at hand (while presumably also allowing the activity to be routed to other brain areas for further processing). Once cued to execute a gaze shift, the activity in the same population rises in a stable manner allowing saccade initiation. Scrambling the population code by either shuffling the activations of individual

neurons at each time point or the temporal sequence of population activity drastically alters the stability profile (EDF 3), further suggesting that the above result is due to the specific temporal structure in the recorded population.

Next, we explored the robustness of the temporal stability hypothesis. Neurons in the rostral SC are tonically active during fixation[17] and burst for small saccades and microsaccades[18], but they reduce their activity during larger movements[17] (Figure 3A,B). Importantly, they also project to the saccade burst generator[19]. Assuming population stability sets part of the input drive to downstream structures, we hypothesized that the temporal structure in rostral SC neurons must decrease during large saccades but remain elevated during fixation, even when a visual burst occurs in other parts of SC and FEF. In other words, we expected the evolution of temporal stability across rostral SC neurons to be the inverse of what occurs in caudal SC - Figure 3C confirms the prediction. Since rostral SC is also known to play a causal role in the generation of microsaccades, we considered whether the population of rostral SC neurons that burst for microsaccades had a stable temporal structure. This was indeed the case, as seen in EDF 4. Thus, the population activity of neurons in rostral SC, including its temporal structure, supplements the pattern in other parts of SC in suppressing and initiating movements. We also examined the stability of the population in the ipsilateral SC with a response field opposite the location of the saccade target (EDF 5). The results were similar to the profile observed for rostral SC, consistent with the idea of reducing the drive from competing neuronal populations. Moreover, pooling neurons in SC and FEF to form a combined population (since they all project to saccade-generating structures) did not impact the main result (EDF 6).

Note that the delayed saccade task is designed to temporally separate the visual and premotor bursts. In the gap task (Figure 3D), in contrast, the two bursts often overlap and saccade reaction times are reduced ("gap effect"[20]); for the subset of movements with the shortest reaction times, the visual and motor bursts merge[20,21] (Figure 3E). As another critical test, we hypothesized that if temporal stability is crucial to movement initiation, the visual burst during the shortest latency saccade trials should have a stable temporal structure. This was indeed the case (Figure 3F), providing additional evidence in support of the stability hypothesis.

Having established that the temporal structures of visual and premotor bursts differ, we sought to identify a mechanism by which downstream neurons could discriminate between stable and unstable population codes. The mere presence of a differential signal does not imply that the brain utilizes that signal in a meaningful manner. In order to provide a framework within which the signal could be used to control behavior, we constructed a rate-based accumulator model that receives input from visuomovement neurons. The accumulator is an abstraction of a neuron receiving population inputs through its network of dendrites (Figure 4A). For simplicity, we assumed that the output firing rate of the neuron is a monotonically increasing function of the net post-synaptic current[22]. How might the population pattern be converted into a signal that initiates a movement only when the pattern being decoded is stable? Heuristically speaking, the decoder should keep track of the short-term history of population activity, use this "memory" to evaluate stability, and respond selectively when the activity pattern is deemed stable over some time scale. We incorporated these requirements in our model by introducing short-term synaptic plasticity in the form of facilitatory connections[23,24] from the input population to the output unit (accumulator), with a Hebbian-like learning rule and leak current. Since the network only contained excitatory connections, we also included weight normalization to prevent unbounded accumulation in the output (Online Methods and Supplementary Info).

We then tested whether the leaky accumulator with facilitation (LAF) model could exploit temporal structure by feeding it population activity from visuomovement neurons (only inputs from SC shown here, Figure 4B1). We focused on two snippets of activity - the 180 ms period ending at the peak of the visual response, and the 180 ms period terminating 35 ms before saccade onset (when the mean activity in the premotor burst reached a level similar to the peak visual response). To discount effects of the mean firing rate, we matched the population means at each time point by scaling the population vector of one set of inputs by the running ratio of their respective means (Figure 4B2). Note that the temporal structure is preserved in each signal (Figure 4B3). The accumulator increased its activity at a faster rate in response to the stable pattern compared to the unstable pattern (Figure 4B4), suggesting that the network was able to discriminate between two types of population patterns even though the net input drive was identical.

How critical is facilitation to this function? Like the inputs themselves, the weights also showed greater fluctuation during the visual burst (around t=140 ms in red traces, Figure 4B5). Consistent with our heuristic, the weights tracked the input rates when the input was stable, but this correlation dropped away when the input was unstable (Figure 4B6). Note that the shape of the correlation profile is not unlike the stability profile in Figure 4B3. Therefore, facilitation allows the weights to retain the memory of a pattern over the time scale of tens of milliseconds, but the memory can be scrambled by a fluctuating input pattern. We quantified the network's ability to discriminate between the two patterns with a pattern sensitivity index (Figure 4B7). The results here suggest that the accumulator is driven more strongly by the stable premotor burst, even when other features of population activity remain the same.

Neurons in premotor structures are constantly bombarded with information from thousands of presynaptic neurons that are active during sensorimotor processing. It is unclear how activity relevant for movement initiation is discriminated from activity related to other processing. A canonical model of movement initiation, especially in the oculomotor system, is threshold-based gating[4]. Current knowledge points to a role by the omnipause neurons (OPNs) in defining the threshold and controlling saccade initiation[4,25]. However, thresholds vary across behavioural paradigms[12], raising the question of how the threshold is set in a particular condition. Furthermore, evidence that the threshold changes during the course of a trial purely based on OPN activity is limited[25]. A related explanation is that a movement is initiated only when movement-related neurons are active, but most neurons in sensorimotor structures likely span a continuum between having visuomovement activity to pure movement activity[1]. Other models posit that a movement is initiated when neural activity traverses certain optimal regions of the population state space[6] and is inhibited otherwise[7]. While the optimal subspace and nullspace hypotheses are certainly appealing, a mechanistic understanding of why certain patterns of activity translate to movement commands is lacking. We reason that for a decoder downstream, it is important to ensure the stability - or consistency over time - of the input code before processing it to influence output. Population activity that creates a high firing rate drive but is inconsistent should be prevented from triggering a movement. This requirement is critical especially in the case of ballistic movements such as saccades, where the ability to reverse the decision once the movement has been initiated is limited.

Our findings are closely related to the premotor theory of attention[11] and offer a way to reconcile the attention-or-intention debate. They could also account for the mirror-like activity recorded during both action observation and execution in neurons known to project directly to motoneurons in the spinal

cord[26]. In both cases, it is unclear how the same neuronal population represents two distinct signals that serve different functional roles. Our results suggest that this multiplexing ability may be provided by the distinct temporal structures of population activity patterns. Previous studies have looked at the role of precise synchronization in the timing of incoming spikes in the transmission of information and the efficacy of driving the recipient neuron[27,28]. However, input firing rates may vary greatly across the population, limiting the ability to compare to spike times. Our study proposes a mean-field equivalent to the spike-based temporal or correlation code[29,30] by looking at the temporal structure of population firing rates, thus tying together the notion of rate, temporal, and population codes. We suggest that temporal structure of population activity is a critical to understanding movement generation as well as, more broadly, all neuronal communication and its relationship to behaviour.

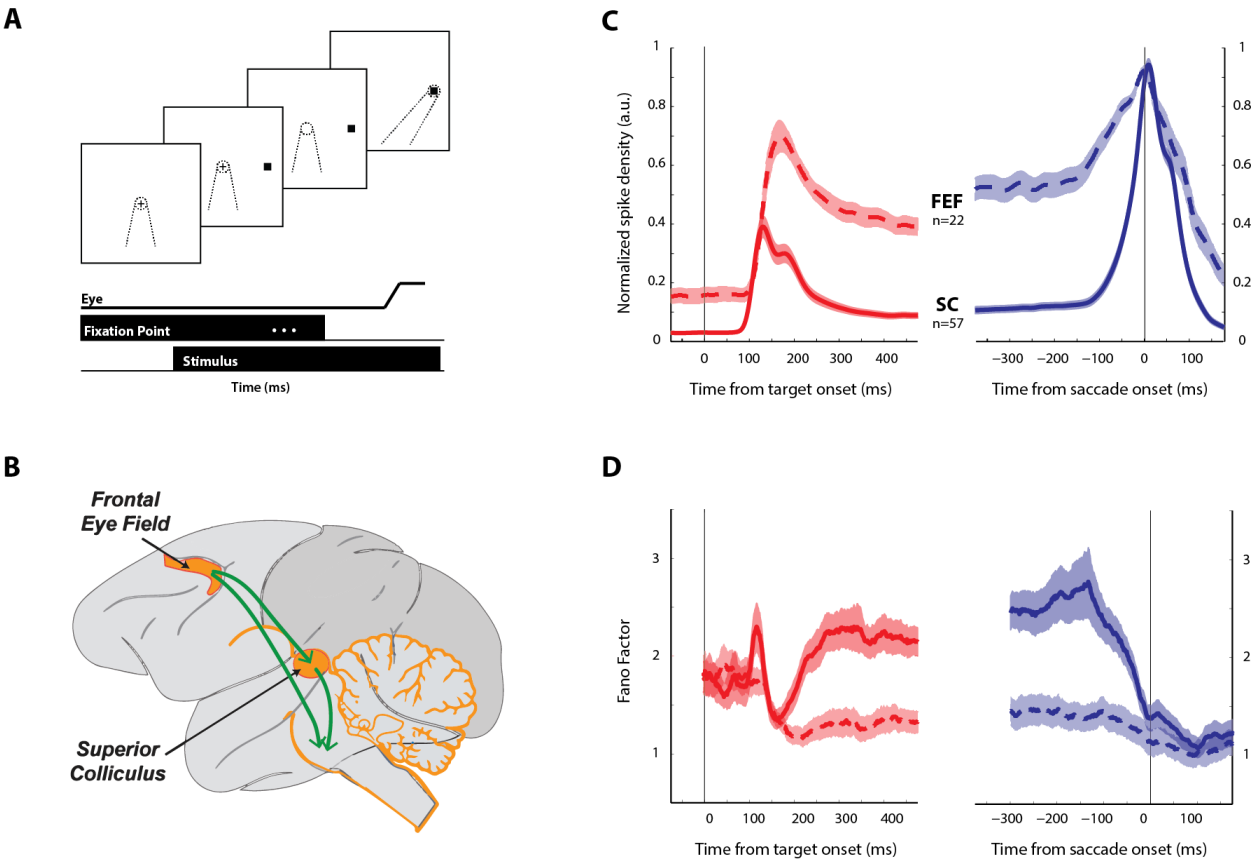

Figure 1. **Sensorimotor transformations are mediated by neurons that multiplex sensory and motor information.** A. Sequence of events in the delayed saccade task. The top panel shows a typical display sequence and the bottom panel shows the timeline. The fixation target is shown as a plus symbol for illustration purposes. Dotted lines depict line of sight of the animal. B. Schematic of the monkey gaze control network showing projections from the FEF and SC to the saccade burst generators in the pons. C. Normalized mean population activity of visuomovement neurons recorded in the SC (solid) and FEF (dashed) during the delayed saccade task. Since SC neurons have firing rates ranging from less than 100 spikes/s to 800 spikes/s, we normalized the spike density of each neuron by its peak magnitude to enable meaningful averaging across the population, mainly for display purposes. The left panel shows data aligned to the onset of the target. The right panel shows data aligned to saccade onset. This colour scheme (red and blue for the two alignments respectively) will be followed throughout the article. Shaded regions indicate s.e.m. D. Fano factor averaged across the population of SC and FEF neurons. Line types/colour scheme same as in C.

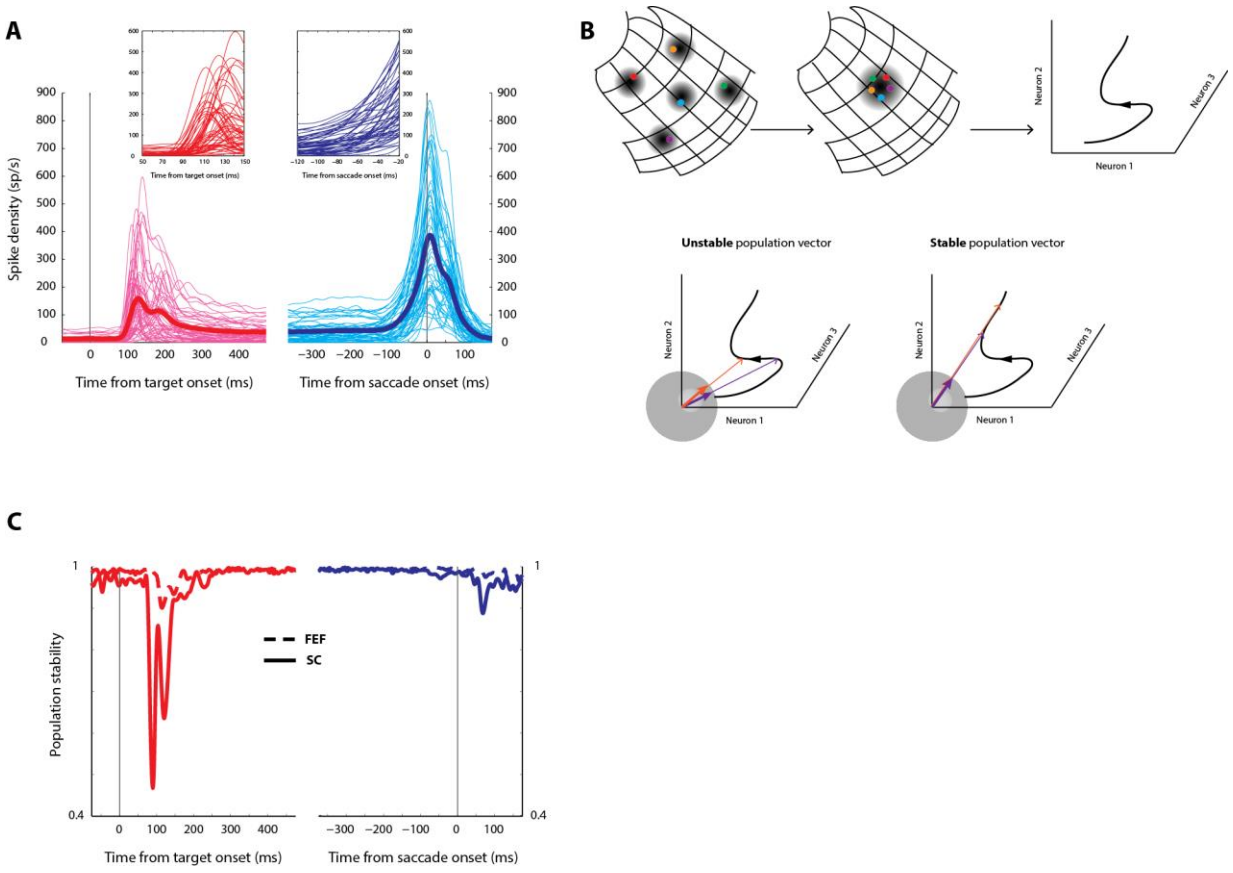

Figure 2. **Population activity is temporally unstable in the visual burst and stable in the motor burst.** A. Activity profiles of individual SC neurons (thin lines) with the population mean (thick line) overlaid. The zoomed in insets highlight the temporal structure of the two bursts. B. Inferring population dynamics from single-unit recordings. The top row depicts the procedure of combining recordings made in different active populations on the SC map (left) into one pseudo-population (middle) that is active for any saccade, enabling the construction of an expected population trajectory (right) in neural state space. The bottom row shows examples of stable and unstable parts of the trajectory. Note that in both cases, the two population vectors (thin arrows in orange and purple) are separated by a similar length of time. In the unstable case, the normalized vectors (thick arrows) move around on the surface of the hypersphere, whereas in the stable case, they stay pointed roughly in the same direction. C. Temporal stability is computed as a dot product between two population vectors separated by tau=20 ms for SC and FEF. Line types as in Figure 1. Population stability shows a drastic reduction at the time of the visual burst, but is stable before and during the onset of the movement.

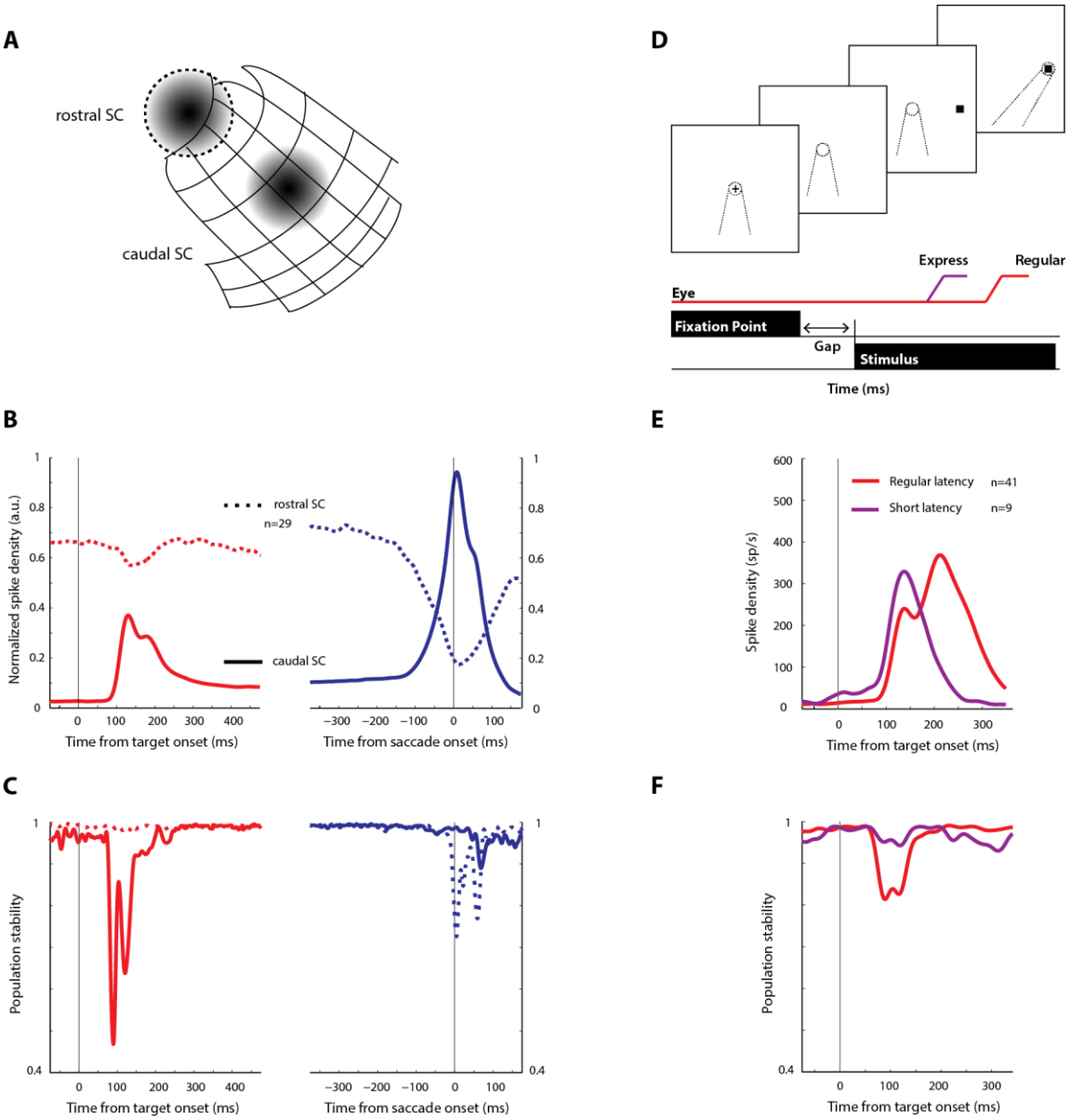

Figure 3. **The stability hypothesis is validated for other neural populations and tasks.** A. Schematic of the SC depicting active populations in the rostral (dotted boundary) and caudal SC (plain). B and C. Normalized activity and temporal stability of the rostral SC population (dotted) with the caudal population shown for comparison. D. Timeline of the gap task with a schematic of regular (red) and express (purple) saccades. E. Mean population activity in caudal SC during the gap task for regular and express-like short latency saccades (colours as in D). Since this is a reactive task, saccade onset is separated from target onset only by 100-200 ms. Data are therefore only shown aligned on target onset for the sake of simplicity. Note the single peak in the burst for the short latency saccades. F. Temporal stability during regular and short latency saccades.

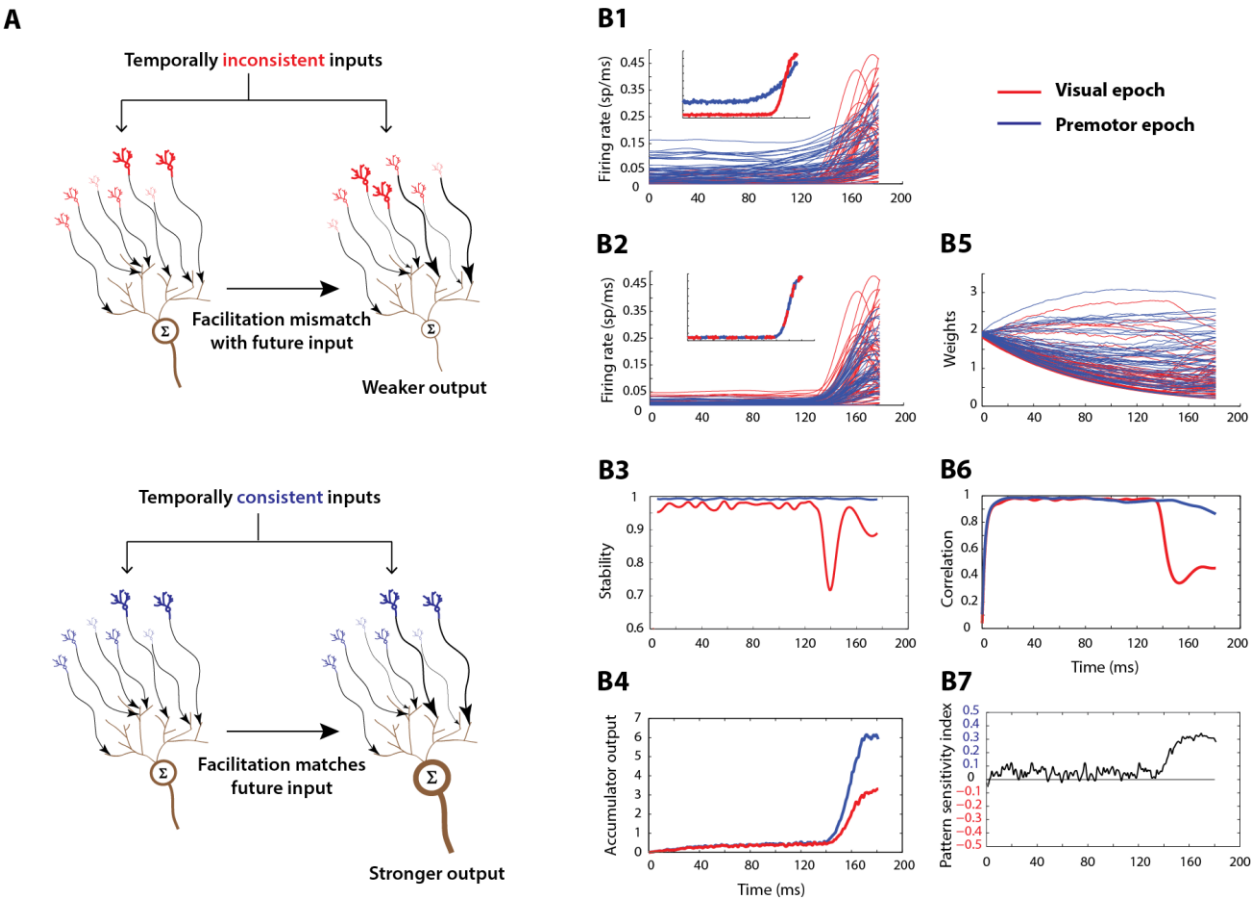

Figure 4. **Leaky accumulator with facilitation model can discriminate population temporal structure.** A. Schematic of the LAF model. The model incorporates a neuron that receives population inputs through its dendritic network and integrates them to produce an output. Each input neuron's activation level is represented by its size and thickness, and its connection strength to the accumulator is represented by the thickness of the arrow. The synaptic weights can grow over time due to short-term facilitation. Two time points are shown for illustration (left – arbitrary initial point, right – subsequent time point). Top – Unstable inputs lead to a scenario where the facilitated synapses that are no longer driven by the strong inputs that created them, whereas, bottom – stable inputs lead to matched strong input and synapses, resulting in stronger accumulation. B. Inputs to the model from SC visuomovement neurons. 1 - Raw unstable (red) and stable (blue) input profiles (inset – population means). The two sets of inputs are 180 ms snippets taken from the visual and premotor bursts, respectively, in the spike density profiles shown in Figure 1. 2 - Mean-matched input profiles and population means. 3 - Temporal stability of the two mean-matched populations. 4 - Output of the LAF accumulator in response to the stable and unstable model inputs. 5 - Evolution of synaptic weights for the two conditions. 6 - Correlation between instantaneous weights and input rates for the two conditions. 7 – Pattern sensitivity index of the model's ability to discriminate between the two types of inputs. Values in the top half of the plot indicate higher sensitivity (faster accumulation) to stable population input.

Methods

General and surgical procedures

All experimental and surgical procedures were approved by the Institutional Animal Care and Use Committee at the University of Pittsburgh and were in compliance with the US Public Health Service policy on the humane care and use of laboratory animals. We used three adult rhesus monkeys (*Macaca mulatta*, 2 male, ages 8 and 6, and 1 female, age 10) for our experiments. Both SC and FEF were recorded in monkey BB whereas only one of either SC or FEF was recorded in monkeys WM and BL, respectively. Under isoflourane anaesthesia, recording chambers were secured to the skull over craniotomies that allowed access to the SC and FEF. In addition, posts for head restraint and scleral search coils to track gaze shifts were implanted. Post-recovery, the animal was trained to perform standard eye movement tasks for a liquid reward.

Visual stimuli and behaviour

Visual stimuli were displayed either by back-projection onto a hemispherical dome (monkeys BB and WM), or on a LED-backlit flat screen television (monkey BL). Stimuli were white squares on a dark grey background, 4x4 pixels in size and subtended approximately 0.5° of visual angle. Eye position was recorded using the scleral search coil technique, sampled at 1 kHz. Stimulus presentation and the animal's behaviour were under real-time control with a Labview-based controller interface[31]. All monkeys were trained to perform standard oculomotor tasks. In the delayed saccade task, the monkey was required to initiate the trial by acquiring fixation on a central fixation target. Next, a target appeared in the periphery but the fixation point remained illuminated for a variable 500-1200 ms, and the animal was required to delay saccade onset until the fixation point was extinguished (GO cue). In the gap task, initial fixation on a central target was followed by a gap period (200 ms) during which the fixation point disappeared, while the animal was required to maintain fixation at the now empty location. This was followed by the appearance of a saccade target in the periphery which was also the GO cue for the animal to make a saccade. All animals performed these tasks with >95% accuracy. Incorrectly performed trials were removed from further analyses. The delayed and gap saccade tasks were occasionally interleaved with visual search paradigms used for a different study. The gap task, when performed in isolation with predictable spatial and temporal features, is often characterized by a bimodal distribution of saccade reaction times (SRTs) with a proportion of saccades occurring at significantly short latencies[32]. Since we interleaved several behavioral tasks, the animal was prevented from constantly being in "gap task mode", and the bimodality of the SRT distribution was not as noticeable. Hence, we divided the gap task trials into two sets based on SRT and labelled the set with shorter SRTs "short latency" saccades (100-150 ms) and the other set as "regular" saccades (170-250 ms). The temporal features of the visual and motor bursts in SC neurons during the short latency trials resembled the profiles observed during express saccades[21].

Electrophysiology

During each recording session, a tungsten microelectrode was lowered into the FEF or SC chamber using a hydraulic microdrive. Neural activity was amplified and band-pass filtered between 200 Hz and 5 kHz and fed to a digital oscilloscope for visualization and spike discrimination. A window discriminator was used to threshold and trigger spikes online, and the corresponding spike times were recorded. Both SC and FEF were confirmed by the presence of visual and movement-related activity as well as the ability to evoke fixed vector saccadic eye movements at low stimulation currents (20-40 uA, 400 Hz, 100 msec). Before beginning data collection for a given neuron, its response field was roughly estimated. In most cases, during collection of data, the saccade target was placed either in the neuron's response field or at the diametrically opposite location in a randomly interleaved manner. In addition, the simulation-evoked saccades were recorded to identify the response field centers (or "hotspots") for the cells recorded during that session. For recordings in rostral SC, stimuli were presented at one of four locations at an eccentricity sufficient to induce a reduction in activity during the large amplitude saccade.

Data analysis and pre-processing

Data were analyzed using a combination of in-house software and Matlab. Eye position signals were smoothed with a phase-neutral filter and differentiated to obtain velocity traces. Saccades were detected using standard velocity criteria. The animal was considered to be maintaining fixation if the gaze remained within a 2-3° window around the fixation target. We also detected any microsaccades that occurred during the delay period in each trial by using a velocity criterion based on the noise in the velocity signal for that trial. Only one of the two monkeys (WM) in whom we recorded neural activity in the rostral SC made sufficient number of microsaccades to permit further analysis.

Raw spike density waveforms were computed for each neuron and each trial by convolving the spike trains with a Gaussian kernel (width = 4ms; in some instances, we used 10 ms for display purposes only). The spike densities were averaged across condition-matched trials (same target location) following alignment with target or saccade onset. We refer to this averaged spike density function for the i^{th} neuron as $R_i(t)$ below. Since SC neurons have firing rates ranging from less than 100 spikes/s to 800 spikes/s (Figure 2A), we also normalized the average spike density of each neuron by its peak magnitude to enable meaningful averaging across the population, mainly for display purposes (e.g., Figure 1C). Neurons were classified as visuomovement neurons if the spike density was significantly elevated above baseline during the visual epoch (50-200 ms following target onset) and during the premotor epoch (50 ms before and after saccade onset). This classification yielded our data set of 57 neurons in caudal SC and 22 neurons in FEF. In addition, rostral SC neurons were defined as fixation-related if the activity during the premotor epoch of large saccades was significantly reduced below baseline (29 neurons). A subset of these neurons also elevated their discharge around the onset of microsaccades (7 neurons). To minimize the effect of noise in the spike density waveforms due to insufficient number of trials in our analysis, we used only neurons which had at least 10 trials for a given condition. This was not a factor in most conditions (we typically had 50-100 trials) except in the case of the gap task. Applying this minimum number of trials criterion resulted in 9 neurons for the short latency condition and 41 neurons for the regular latency condition.

We also computed the Fano factor - the spike count variance across trials divided by the mean spike count - for each neuron in the delayed saccade task. Spikes were counted in 100 ms windows sliding in increments of 1 ms. The Fano factor trace was then shifted forward in time by half the window size (50 ms). The rationale behind this correction is that the beginning of any change in the spike count statistics at a given time t is going to be captured in a window centered at t-50 ms. The Fano factor was then averaged across neurons to obtain a population trace (Figure 1D).

Inferring population dynamics from single-unit recordings

Our analyses and results build on the ability to infer features of population dynamics from single-unit activity profiles recorded sequentially over multiple sessions. In order to do this, we constructed a simulacrum of the population activity in SC and FEF by combining all of our single-unit recordings. We define $\mathbf{R}(t)$ as a population activity vector:

$$\mathbf{R}(t) = \begin{bmatrix} R_1(t) \\ R_2(t) \\ \dots \\ R_n(t) \end{bmatrix}$$

where $\mathbf{R}(t)$ represents the instantaneous activity at time t as a point in an *n*-dimensional space, where *n* is the number of neurons in the population. The curve connecting successive points over time is the neural trajectory that describes the evolution of population activity. Note that each neuron's firing rate waveform $R_i(t)$ is the average across many matched trials (identical stimulus/response conditions). Thus the neural trajectory is the *expected trajectory* of population activity. Since these neurons have a fairly broad RF, many neurons constitute the active population for any given visual stimulus or saccade[33]. Our neurons were sampled roughly (but not exactly) around the hotspot of the active population for a given session. Therefore, the pooled data from individual sessions can be thought of as an approximation of the population mound active for an arbitrary location/RF in the visual field on any given trial. Many recent studies have reconstructed such "pseudo-populations" from sequentially recorded neurons[34-36] and found comparable properties from simultaneous and serial recordings[7]. Indeed, this is also expected of our pseudo-population under the assumption of isotropy – that each neuron's contribution to its respective local active population is similar regardless of the locus of the population. To better demonstrate this, we estimated the location of a given neuron in the active pseudo-population as follows (we use SC for illustrative purposes because of its convenient topography). We used the point image of the target location on the SC map as a representation as the center of the active population for that session, and used the stimulation-evoked saccade vector to identify the location of that neuron on the SC. We referenced the point image of each target location to a single location to create an active pseudo-population and translated the neuron locations relative to this population center (EDF 1). All mathematical equations for transforming between visual and SC tissue coordinates have been defined previously[37]. Inclusion of stimuli/saccades in the anti-preferred RF of the neurons allowed us to also estimate a pseudo-population of neurons in the ipsilateral SC. To complete the representation of activity across the SC topography, we also recorded from and included in our analyses neurons in the rostral portion of SC, which are active during fixation, burst during

microsaccades, and are suppressed during large saccades. Moreover, to account for correlations between neurons on individual trials (noise correlation), we show that the temporal stability profile derived from the across-trial mean population dynamics (see next section) is a theoretical upper bound on the stability expected on single trials (Supplementary Material and EDF 1). The findings in this letter are therefore independent of our methodological assumptions and are robust in the face of correlations within the population. It is also important to emphasize that these results are also independent of any across-trial jitter in the phase of the display system's refresh cycle since we use the trial-averaged neural activity for all our analyses.

Temporal stability analysis

To assess temporal stability, we first normalized the population trajectory $\mathbf{R}(t)$ by its Euclidean norm ($\|\mathbf{R}(t)\|$), equivalently its magnitude, at each time point to yield $\widehat{\mathbf{R}}(t)$*:*

$$\widehat{\mathbf{R}}(t) = \frac{\mathbf{R}(t)}{\|\mathbf{R}(t)\|}$$

The normalized trajectory can be visualized as a unity length population vector that points in an n-dimensional direction at each instant in time. That is, while $\mathbf{R}(t)$ is free to traverse the n-dimensional activity space, $\widehat{\mathbf{R}}(t)$ is constrained to the surface of an n-dimensional hypersphere (Figure 2B). Temporal stability or consistency of the evolving population was then quantified by the dot product of two time-shifted unity length vectors:

$$S(t) = \widehat{\mathbf{R}}(t-\tau) \cdot \widehat{\mathbf{R}}(t+\tau)$$

The stability metric ($S(t)$) tracks the running similarity of the normalized trajectory separated in time by 2τ msec. Crucially, the normalization constrains $S(t)$ between 0 and 1. Thus, if $S(t) \to 1$, the population activity is considered stable since the relative contribution of each neuron is consistent. If $S(t) \ll 1$, the population activity is deemed unstable because the relative contribution is variable. If the neural trajectory is not normalized, the dot product quantifies similarity across the vectors' magnitude and direction. It roughly mimics the quadratic of the firing rate (exactly so for τ=0). When the vector direction remains constant, the dot product yields no additional information than that already present in the firing rate. In contrast, the normalization scales the neural trajectory so it always has unity magnitude. It neither alters the relative contributions of the neurons nor compromises the vector direction. The dot product therefore performs an unbiased evaluation of stability based only on vector direction, and is an estimate of the fidelity of the population code modulo a multiplicative gain factor. Intuitively, the stability measure is analogous to the correlation between the neurons' activities at two different time points. We chose the dot product, however, because of its interpretability as a measure of pattern similarity in n-dimensional activity space.

Since temporal stability is defined over the whole population and gives rise to a singular measure at a given time, it is not directly amenable to statistical significance analysis. Therefore, we took an alternative approach in order to ensure that the observed stability profiles were contingent on the recorded activity. We shuffled the population activity in two different ways and bootstrapped the stability across multiple shuffles for each type of shuffle (EDF 3). First, we shuffled the activity by randomly assigning each vector in the set of population vectors across time to different time points. This

temporal shuffle retains each neuron's identity in the population but scrambles the structure across time. Next, we randomly shuffled the neuron's activities at each time point. This shuffle retains the average firing rate at each instant but removes any temporal correlation in the firing rate across neurons. We performed multiple shuffles of each kind and computed temporal stability for each instance to obtain bounds for the stability profile in the original data.

Leaky accumulator with facilitation (LAF) model

We developed a computational model to demonstrate how the temporal structure of population activity could be used by neural circuits to gate decisions such as movement initiation. The core idea behind the model is the hypothesis that signal integration is stronger when the temporal structure in input activity is stable, which allows the decoder neuron to reach threshold during the high frequency burst that triggers the movement. We constructed an accumulator as an abstraction of a neuron receiving population inputs through its network of dendrites. The total synaptic current ($I(t)$) and the firing rate ($v(t)$) of the accumulator were defined as

$$\tau_s \dot{I} = -I + \sum_1^n w_i u_i$$

and

$$v = F(I)$$

where u_i and w_i are the instantaneous firing rate and synaptic gain of the i^{th} input neuron, and τ_s is the time constant of the synaptic current. The output firing rate of the single decoder neuron ($v(t)$) can be described by a standard monotonic function (e.g., linear or sigmoid) applied to the net current. The family of stochastic, leaky accumulator models that integrate the firing rate of neurons toward a threshold criterion has been commonly used to explain reaction time, decision making, and perception (*refs*). We used the following heuristic in order to extend this framework to incorporate temporal structure. In order to assess stability, the decoder neuron must keep track of the short term history of the population activity, use this "memory" to evaluate stability, and respond selectively when the activity pattern is deemed stable over some time scale. We implemented these requirements by introducing short-term plasticity in the form of facilitatory connections from the input population onto the output unit (accumulator). The change in connection strength or gain of each neuron on the decoder neuron (w_i) can be defined by a differential equation that incorporates a Hebbian-like learning rule and leak current:

$$\tau_w \dot{w}_i = -w_i + \frac{u_i v}{w n f_i}$$

The Hebbian-learning component, ($u_i v$) describes the change in weight coupled to the firing rates of the i^{th} pre-synaptic neuron and the post-synaptic accumulator neuron. τ_w is the time constant of the weight parameter. Since this version of the model contains only excitatory connections, the weight parameter can exhibit unbounded accumulation, which can be controlled by incorporating normalization. We normalized the Hebbian-learning component ($u_i v$) with the contribution of that neuron to the total resource pool. The resource pool available for facilitation at any given time was defined as the sum of the Hebbian-learning component across all input units ($\sum_1^n u_i v$). The contribution of a neuron to the

output rate v then determines its contribution to the overall pool, giving rise to the weight normalization factor:

$$\mathrm{wnf_i} = \sum_{1}^{n} \mathrm{u_i w_i u_i}$$

For the model simulation, we used visuomovement neuron population activity in SC as inputs. We created two sets of input snippets from the visual and premotor bursts, each 180 ms in length. For the visual burst, we used the activity upto the peak in the population response. For the premotor burst, we used activity upto 35 ms before saccade onset, when the response magnitude reached the same level as the peak of the visual burst. In order to control for the effect of average firing rate on the accumulation, we mean-matched the input profiles as follows. We divided the activations in the premotor input set at each instant by the mean activation of the visual inputs at the corresponding instant. That is,

$$\mathrm{u_i^{pre}(t)_{mm}} = \frac{\mathrm{u_i^{pre}(t)}}{\frac{1}{n}\sum_1^n \mathrm{u_i^{vis}(t)}}$$

where $\mathrm{u_i^{vis}(t)}$ and $\mathrm{u_i^{pre}(t)}$ are the activity of neuron i at time t in the visual and premotor input sets, respectively, and $\mathrm{u_i^{pre}(t)_{mm}}$ is the premotor input instantaneously rescaled to match the mean of the visual input. This ensured that we isolated the effect of temporal structure, independent of firing rate, on the model's response. We also quantified the ability of the synaptic weights to track the inputs by computing the Pearson's correlation between the weight and input vectors at each time point. To quantify the accumulator's ability to discriminate temporal pattern in population input, we computed a pattern sensitivity index (psi) as

$$\mathrm{psi(t)} = \frac{\mathrm{v^{pre}(t) - v^{vis}(t)}}{\mathrm{v^{pre}(t) + v^{vis}(t)}}$$

where v(t) is the output of the accumulation for the corresponding inputs.

Extended Data Figures

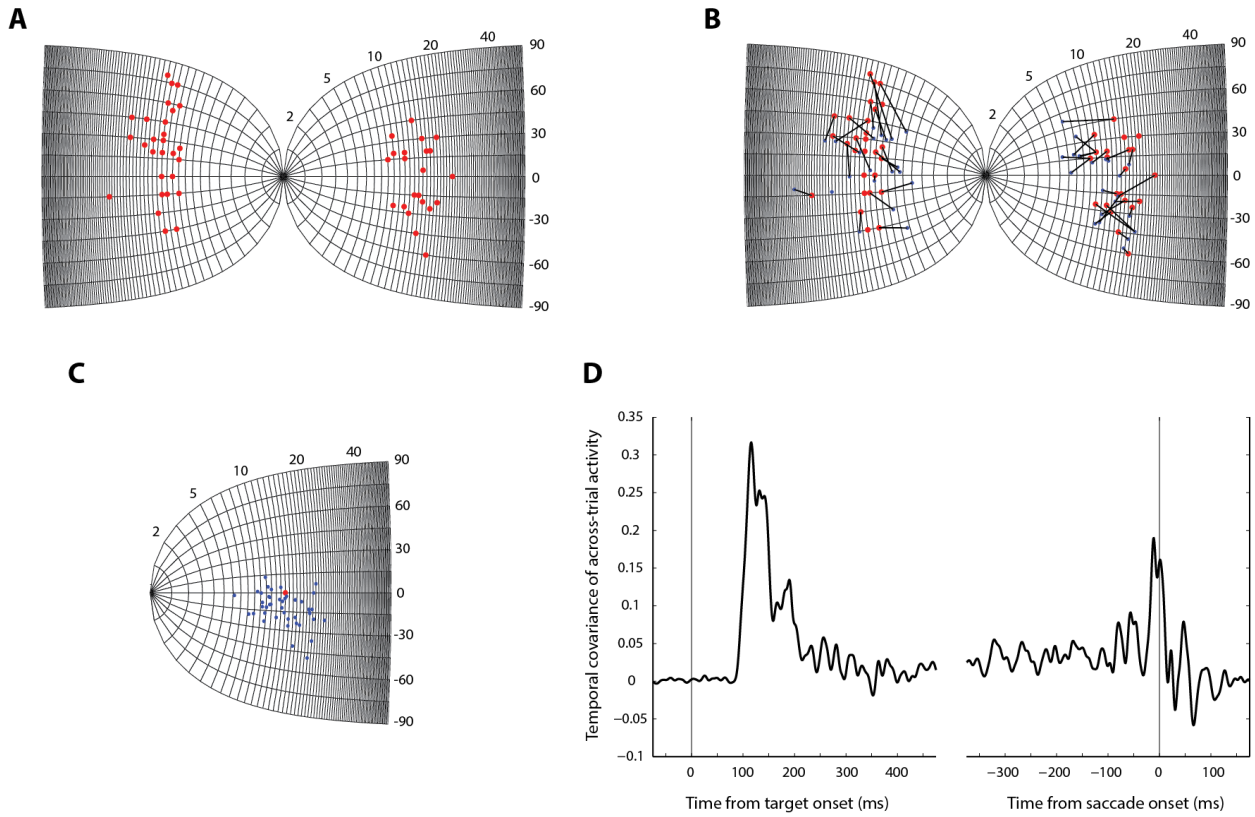

Extended Data Figure 1. Inferring population dynamics from single-unit recordings. A. Point images (red) of target locations on the SC map across all experimental sessions. The locations on the SC were computed using known transformations between visual space and SC tissue coordinates (Online Methods). B. Same as in A, with the endpoint of the stimulation-evoked saccade vector at the recording site shown in blue. The stimulation vector provides a proxy for the RF center of the recorded neuron. Neuron-target pairs (blue-red) from individual sessions are connected using black lines. C. The active pseudo-population on the SC map. The red locations from A and B were referenced to an arbitrary location on the SC map (here, R=15, theta = 0) and the blue locations appropriately translated. Points from both colliculi have been shown on a single SC for the sake of clarity. D. Covariance of activity over time and across trials averaged across all visuomovement neurons in SC aligned on target (left) and saccade (right) onsets. For a derivation of how using the average activity for each neuron sets limits on the expected stability on single trials, see Supplementary Material.

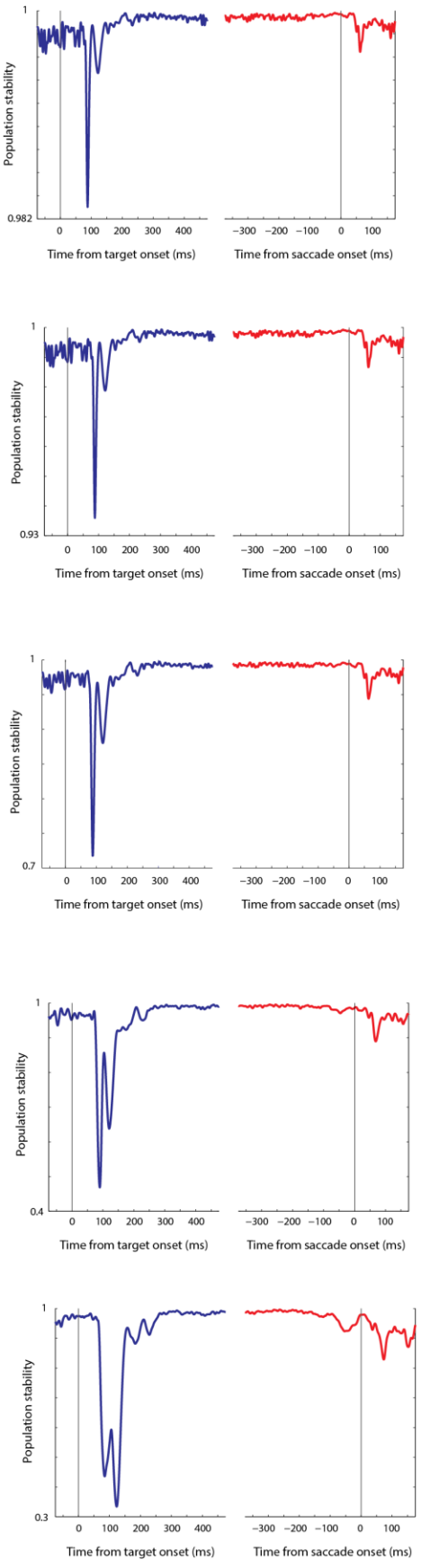

Extended Data Figure 2. Temporal stability as a function of τ. In order to ensure that the choice of τ did not have an undue effect on our results, we computed stability for several values of τ. The panels show temporal stability profiles for SC as in Figure 2C, for (from top to bottom), τ = 1, 2.5, 5, 10, and 20, respectively. As seen, the absolute magnitude of stability was inversely related to τ - a consequence of the smooth and continuous nature of the trajectory. In other words, since the state of the neural population evolves smoothly, it must traverse intermediate states in order to move from one state to another, resulting in greater similarity between state vectors close together in time than those further apart. However, the relative shape of stability profile was largely preserved across τ (except for some deviation for values of τ as high as 40 ms, possibly a consequence of comparing population vectors from different epochs). Thus, the relative instability during the visual epoch and stability during the premotor epoch persists across all time separations.

538

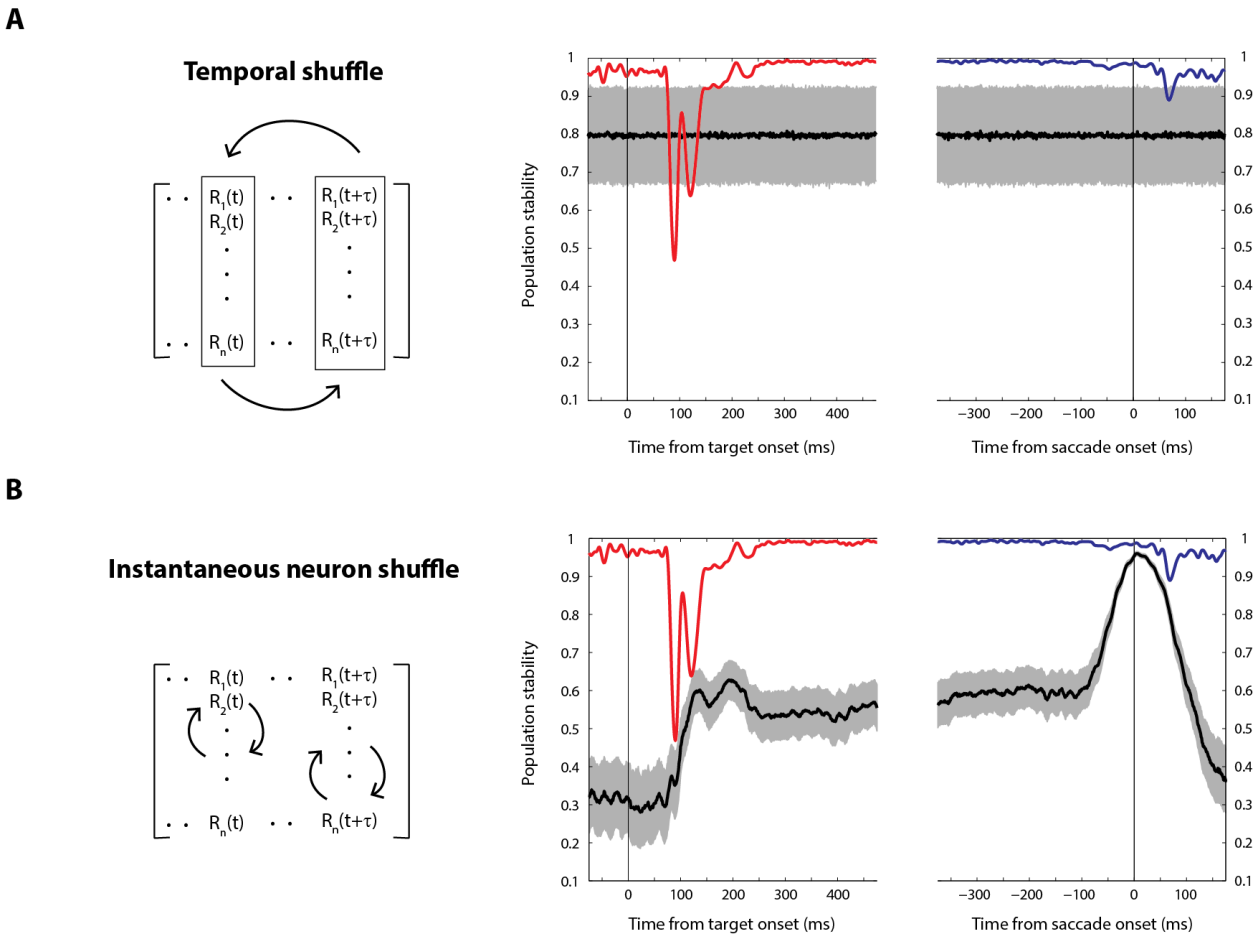

Extended Data Figure 3. Temporal stability profile is specific to the recorded population structure. A. Left - The population code was altered by randomly shuffling the population vectors between different time points, i.e., the activity vectors are taken from the population trajectory in the original data but in a different temporal sequence. Right - The black trace is the mean temporal stability across 1000 shuffles, and the gray region is the standard deviation across these samples. The stability profile flattens at what is effectively the average value of the dot product between any two vectors in the trajectory. This bootstrap approach indicates that the observed stability profile (red and blue traces) is specific to the true population dynamics. B. Left - The population code was scrambled by randomly shuffling the neuron's activities at each time point. This shuffle preserves the average population activity at each instant while removing any ordering between individual neurons. Right - The observed stability profile (red and blue traces) is well outside the distribution of profiles obtained across 1000 shuffles (mean – black trace, standard deviation – gray region).

557

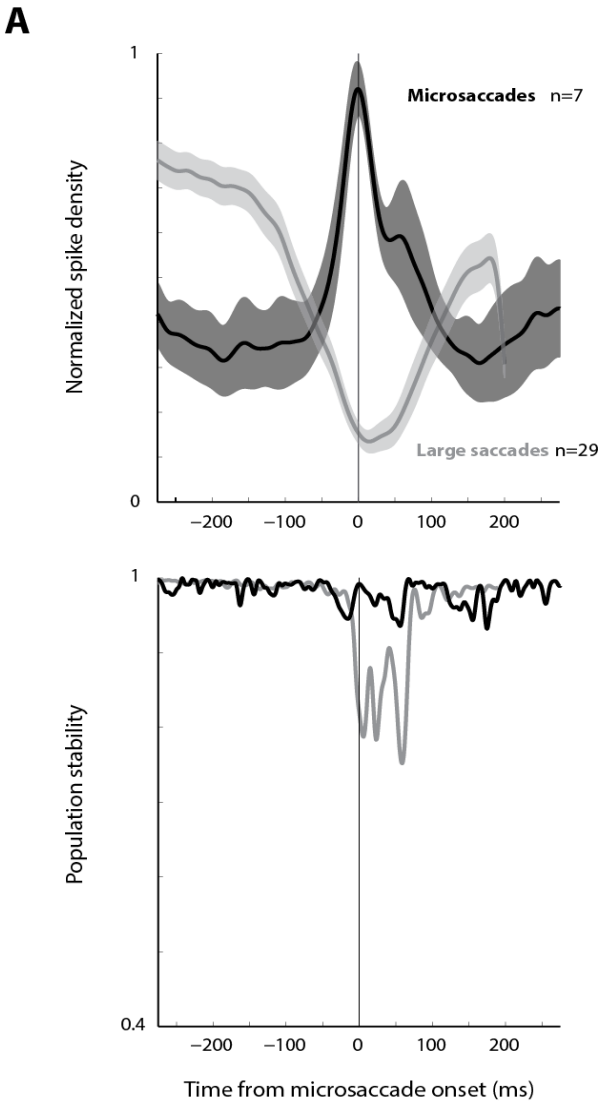

558

559

560 **Extended Data Figure 4. Population activity of rostral SC neurons is stable during microsaccades.** Top –
561 Normalized population activity of microsaccade-related neurons in rostral SC (black). Note the strong
562 burst compared to the suppression in fixation-related neurons in the same region for large saccades
563 (gray). Bottom – Temporal stability of the rostral SC population for microsaccades shown in comparison
564 to large saccades. Neurons which burst for microsaccades remain stable during these fixational eye
565 movements, consistent with the hypothesis that both an increase in firing rate and high stability is
566 required for movement generation.

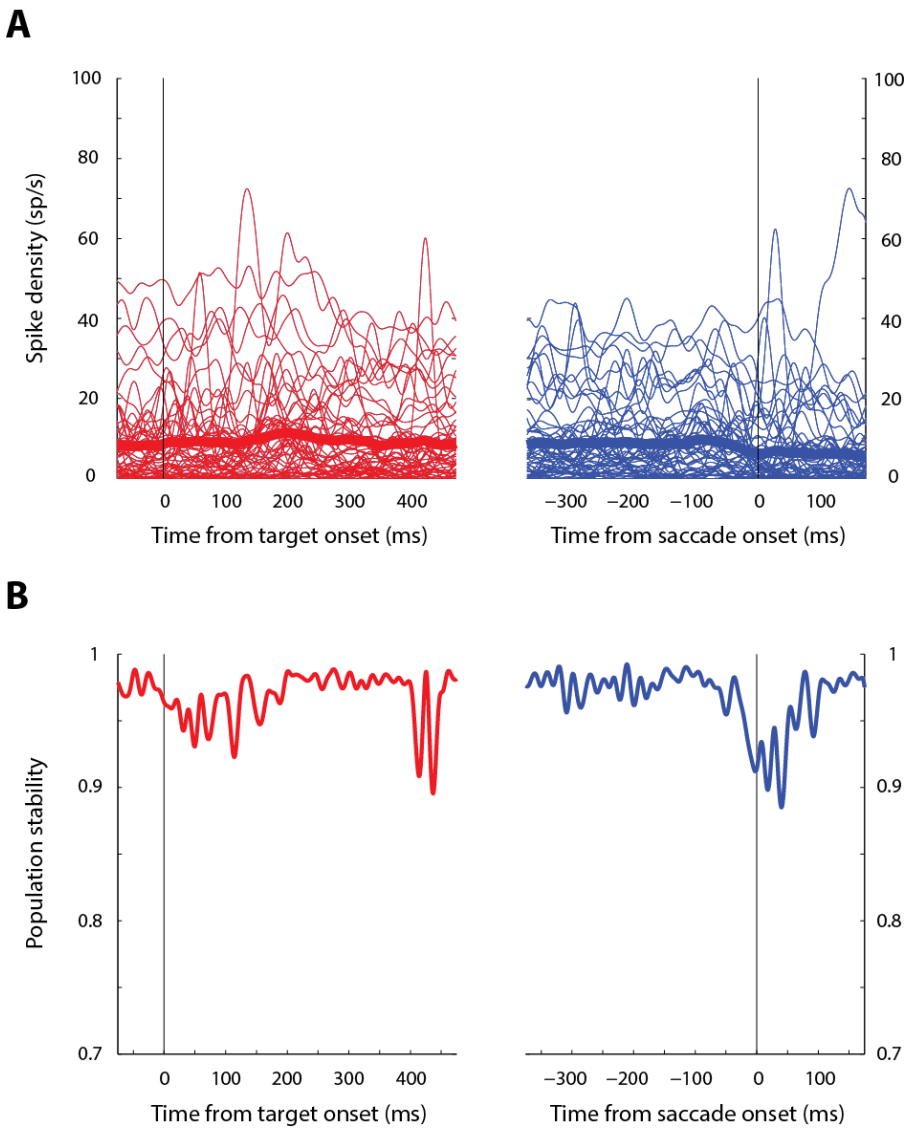

Extended Data Figure 5. Characteristics of the population in ipsilateral SC. A. Spike densities of individual neurons (thin traces) and the population average (thick trace) when the target (left panel) and saccade (right panel) were in the ipsilateral hemifield. These neurons show little to no modulation in their firing rate when neurons in the contralateral SC actively produce bursts. B. Temporal stability of the ipsilateral population aligned on target (left) and saccade (right) onset. Like the rostral SC (Figure 3), the ipsilateral population is relatively more unstable during the saccade, suggesting that stability may be an actively controlled variable designed to reduce the effective drive from competing neuronal populations during movement generation.

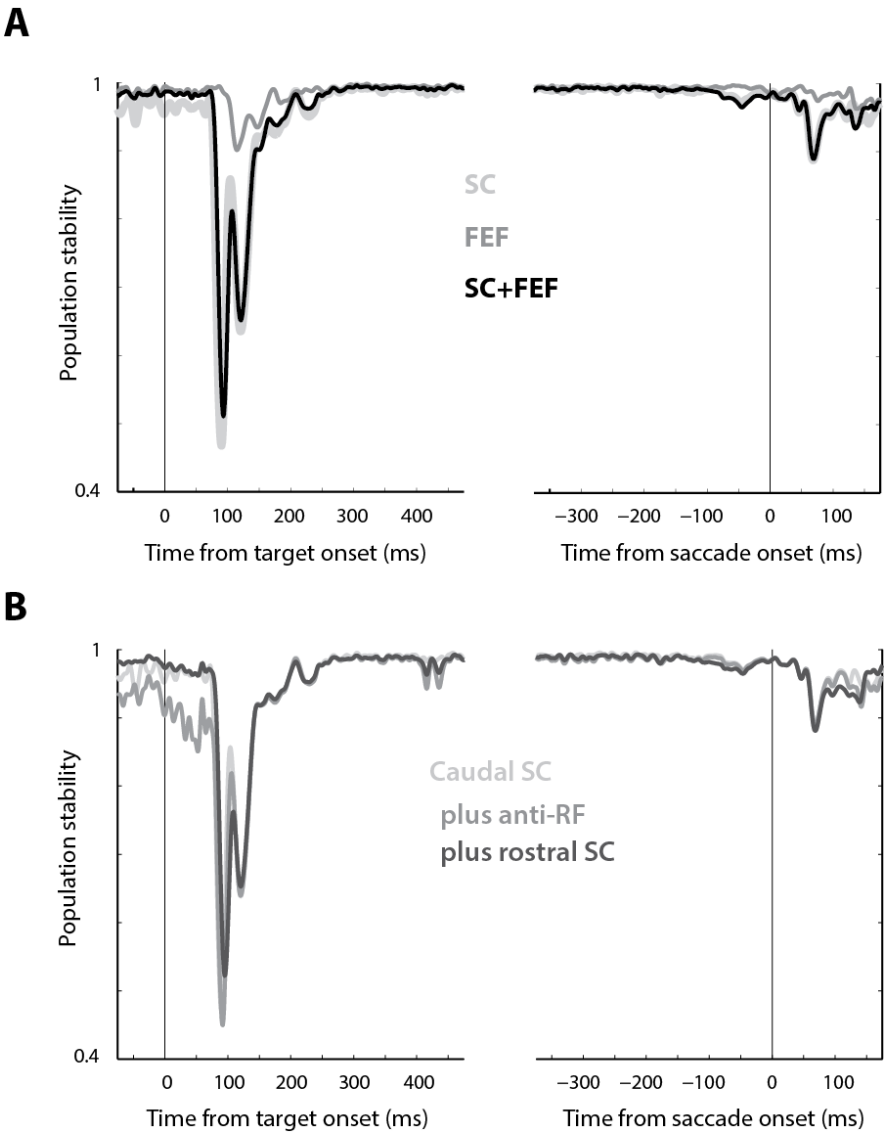

Extended Data Figure 6. Temporal stability of combined populations. A. Temporal stability aligned on target (left) and saccade (right) onset for neurons constituting the individual "active populations" in caudal SC and FEF (same as Figure 2) in the two shades of gray, and the combined active population in black. Since the burst generators receive input from both sets of neurons, it is important to verify that the characteristics of population temporal structure is preserved for the whole population. B. Temporal stability for the active caudal SC population (light gray, same as above and Figure 2), combined caudal SC population (including the ipsilateral SC from EDF4, medium gray), and all neurons in SC (dark gray). Since the ipsilateral and rostral SC populations contribute little to the firing rate vector, their contribution to the dot product is also low – therefore, any difference between these stability profiles is small.

Supplementary text

S1. Inferring population dynamics from single-unit recordings

We previously described in the main text and methods how we reconstructed a pseudo-population from unit recordings. Using knowledge of the RF centre of a given session's local population obtained from microstimulation, and known transformation from visual space to SC tissue coordinates, here we reconstruct the pseudo-population on the SC map.

We first transferred target locations (R_T, θ_T) inside the RF for each neuron onto the SC map using the following transformations[37] –

$x_T = \frac{B_x}{2} \ln \frac{(H+A)^2+V^2}{A^2}$, $y_T = B_y \tan^{-1} \frac{V}{H+A}$, where,

$H = R_T \cos\theta_T$, $= R_T \sin\theta_T$, and $A = 3$, $B_x = 1.4$, $B_y = 1.8$.

The transformed locations (x_T, y_T) on the bilateral SC map are shown in EDF1, panel A. In order to move these target locations to one pseudo-population, we need to identify where these points reside in the RF of each neuron or local population. Previous studies have demonstrated a strong correspondence between the saccade vector evoked by microstimulation and the centre of the RF of neurons at the site of microstimulation. We used the endpoints of the site-specific microstimulation-evoked saccades as a proxy for the respective RF centres. The transformed endpoints, with their locations relative to the corresponding target locations, are shown in EDF1, panel B. We picked an arbitrary location in the visual field as the RF centre of the pseudo-population, $(R_c, \theta_c) = (15,0)$. We used the fact that the size of the active SC population is invariant regardless of the encoded saccade to preserve relative distances in tissue space between a site's target location and RF centre, and translated the transformed microstimulation endpoints to the common pseudo-population centre, along with the respective target locations. To construct one active population from sites gleaned from both hemifields (and therefore both colliculi), we reflected the coordinates from one colliculus onto the other. The resulting pseudo-population (EDF1, panel C) shows a fairly representative sampling of neurons from the pseudo-population, with its extent consistent with a large (25% of SC tissue) active population, albeit one that is biased to one side of the population.

A fundamental assumption behind treating the expected population trajectory as a proxy for an arbitrary single-trial trajectory is that relevant features of single-trial population dynamics are captured by the expected population trajectory. However, it is possible that correlated dynamics between neurons, such as noise correlations on individual trials, may cause measures based on single-trial trajectories to deviate significantly from the dynamics of the average. We show here that our measure of the structure of the trial-specific population code – temporal stability – is indeed preserved in the expected trajectory.

Let us denote by $\hat{R}(t)$ the population unit vectors comprising the expected trajectory. Let us also denote the population unit vectors making up individual trial trajectories by $\widehat{{}_kR}(t)$, where k is a trial index. The expectation of the inner product stability measure across trials is given by,

$$E\left[\widehat{{}_kR}\left(t-\frac{\tau}{2}\right).\widehat{{}_kR}\left(t+\frac{\tau}{2}\right)\right] =$$

630 $$E[\sum_i {}_kR_i(t-\frac{\tau}{2})\ {}_kR_i(t+\frac{\tau}{2})] =$$

631 $$\sum_i E[\,{}_kR_i(t-\frac{\tau}{2})\ {}_kR_i(t+\frac{\tau}{2})] =$$

632 $$\sum_i E[{}_kR_i(t-\frac{\tau}{2})]\,E\,[{}_kR_i(t+\frac{\tau}{2})] - Cov[\,{}_kR_i(t-\frac{\tau}{2}),\,{}_kR_i(t+\frac{\tau}{2})] <$$

633 $$\sum_i E[{}_kR_i(t-\frac{\tau}{2})]\,E[{}_kR_i(t+\frac{\tau}{2})] =$$

634 $$\sum_i R_i\left(t-\frac{\tau}{2}\right)\ R_i\left(t+\frac{\tau}{2}\right) =$$

636 $$\hat{R}\left(t-\frac{\tau}{2}\right).\hat{R}(t+\frac{\tau}{2})$$

635

637 Therefore, $E\left[\widehat{{}_kR}\left(t-\frac{\tau}{2}\right).\widehat{{}_kR}\left(t+\frac{\tau}{2}\right)\right] < \hat{R}\left(t-\frac{\tau}{2}\right).\hat{R}(t+\frac{\tau}{2})$, i.e., the stability profile obtained using
638 individual trial trajectories and then averaging across trials will be lower than that obtained from the
639 expected single-trial trajectory (as we do here). The inequality holds only if the second term in the sum,
640 the covariance between normalized time-separated activity across trials, is positive. Intuitively, this
641 seems likely because of the fact that the activity of these neurons evolves smoothly. We verified this by
642 computing the evolution of temporal covariance across trials for each neuron. Since we do not have
643 access to the population unit vectors for individual trials, we simply used the unnormalized activity,
644 reasoning that covariance should be unaffected by normalization scaling. The average covariance profile
645 is shown in EDF1, panel D. Note that the covariance is largely positive, with minor deviations late during
646 the trial. Importantly, note that the covariance is higher during the visual epoch compared to the
647 premotor epoch. This will produce a greater reduction in stability (step 4 in derivation) during the visual
648 epoch in the true single-trial trajectories, only strengthening our result.

649

650

651

652

653

654

655

656

657

658

References

1 Wurtz, R. H., Sommer, M. A., Paré, M. & Ferraina, S. Signal transformations from cerebral cortex to superior colliculus for the generation of saccades. *Vision Res* **41**, 3399-3412 (2001).

2 Buneo, C. A., Jarvis, M. R., Batista, A. P. & Andersen, R. A. Direct visuomotor transformations for reaching. *Nature* **416**, 632-636 (2002).

3 Gallese, V., Fadiga, L., Fogassi, L. & Rizzolatti, G. Action recognition in the premotor cortex. *Brain : a journal of neurology* **119 (Pt 2)**, 593-609 (1996).

4 Hanes, D. P. & Schall, J. D. Neural control of voluntary movement initiation. *Science* **274**, 427-430 (1996).

5 Keller, E. L. Participation of medial pontine reticular formation in eye movement generation in monkey. *J Neurophysiol* **37**, 316-332 (1974).

6 Churchland, M. M. *et al.* Neural population dynamics during reaching. *Nature* **487**, 51-56 (2012).

7 Kaufman, M. T., Churchland, M. M., Ryu, S. I. & Shenoy, K. V. Cortical activity in the null space: permitting preparation without movement. *Nat Neurosci* **17**, 440-448 (2014).

8 Rodgers, C. K., Munoz, D. P., Scott, S. H. & Pare, M. Discharge properties of monkey tectoreticular neurons. *J Neurophysiol* **95**, 3502-3511 (2006).

9 Segraves, M. A. Activity of monkey frontal eye field neurons projecting to oculomotor regions of the pons. *J Neurophysiol* **68**, 1967-1985 (1992).

10 Kustov, A. A. & Robinson, D. L. Shared neural control of attentional shifts and eye movements. *Nature* **384**, 74-77 (1996).

11 Rizzolatti, G., Riggio, L., Dascola, I. & Umilta, C. Reorienting attention across the horizontal and vertical meridians: evidence in favor of a premotor theory of attention. *Neuropsychologia* **25**, 31-40 (1987).

12 Jantz, J. J., Watanabe, M., Everling, S. & Munoz, D. P. Threshold mechanism for saccade initiation in the frontal eye field and superior colliculus. *J Neurophysiol* **109**, 2767-2780 (2013).

13 Chang, M. H., Armstrong, K. M. & Moore, T. Dissociation of response variability from firing rate effects in frontal eye field neurons during visual stimulation, working memory, and attention. *J Neurosci* **32**, 2204-2216 (2012).

14 Churchland, M. M. *et al.* Stimulus onset quenches neural variability: a widespread cortical phenomenon. *Nat Neurosci* **13**, 369-378 (2010).

15 Steinmetz, N. A. & Moore, T. Changes in the response rate and response variability of area V4 neurons during the preparation of saccadic eye movements. *J Neurophysiol* **103**, 1171-1178 (2010).

16 Churchland, M. M., Yu, B. M., Ryu, S. I., Santhanam, G. & Shenoy, K. V. Neural variability in premotor cortex provides a signature of motor preparation. *J Neurosci* **26**, 3697-3712 (2006).

17 Munoz, D. P. & Wurtz, R. H. Fixation cells in monkey superior colliculus. I. Characteristics of cell discharge. *J Neurophysiol* **70**, 559-575 (1993).

18 Hafed, Z. M., Goffart, L. & Krauzlis, R. J. A neural mechanism for microsaccade generation in the primate superior colliculus. *Science* **323**, 940-943 (2009).

19 Moschovakis, A. K., Scudder, C. A. & Highstein, S. M. The microscopic anatomy and physiology of the mammalian saccadic system. *Progress in neurobiology* **50**, 133-254 (1996).

20 Dorris, M. C. & Munoz, D. P. A neural correlate for the gap effect on saccadic reaction times in monkey. *J Neurophysiol* **73**, 2558-2562 (1995).

21 Edelman, J. A. & Keller, E. L. Activity of visuomotor burst neurons in the superior colliculus accompanying express saccades. *J Neurophysiol* **76**, 908-926 (1996).

22 Rauch, A., La Camera, G., Luscher, H. R., Senn, W. & Fusi, S. Neocortical pyramidal cells respond as integrate-and-fire neurons to in vivo-like input currents. *J Neurophysiol* **90**, 1598-1612 (2003).

23 Tsujimoto, T., Jeromin, A., Saitoh, N., Roder, J. C. & Takahashi, T. Neuronal calcium sensor 1 and activity-dependent facilitation of P/Q-type calcium currents at presynaptic nerve terminals. *Science* **295**, 2276-2279 (2002).

24 Borst, J. G. & Sakmann, B. Facilitation of presynaptic calcium currents in the rat brainstem. *The Journal of physiology* **513 (Pt 1)**, 149-155 (1998).

25 Everling, S., Paré, M., Dorris, M. C. & Munoz, D. P. Comparison of the discharge characteristics of brain stem omnipause neurons and superior colliculus fixation neurons in monkey: implications for control of fixation and saccade behavior. *J Neurophysiol* **79**, 511-528 (1998).

26 Vigneswaran, G., Philipp, R., Lemon, R. N. & Kraskov, A. M1 corticospinal mirror neurons and their role in movement suppression during action observation. *Curr Biol* **23**, 236-243 (2013).

27 Carter, A. G., Soler-Llavina, G. J. & Sabatini, B. L. Timing and location of synaptic inputs determine modes of subthreshold integration in striatal medium spiny neurons. *J Neurosci* **27**, 8967-8977 (2007).

28 Branco, T., Clark, B. A. & Hausser, M. Dendritic discrimination of temporal input sequences in cortical neurons. *Science* **329**, 1671-1675 (2010).

29 Softky, W. Sub-millisecond coincidence detection in active dendritic trees. *Neuroscience* **58**, 13-41 (1994).

30 Harvey, M. A., Saal, H. P., Dammann, J. F., 3rd & Bensmaia, S. J. Multiplexing stimulus information through rate and temporal codes in primate somatosensory cortex. *PLoS biology* **11**, e1001558 (2013).

31 Bryant, C. L. & Gandhi, N. J. Real-time data acquisition and control system for the measurement of motor and neural data. *J Neurosci Methods* **142**, 193-200 (2005).

32 Fischer, B. & Boch, R. Saccadic eye movements after extremely short reaction times in the monkey. *Brain Res* **260**, 21-26 (1983).

33 Sparks, D. L., Holland, R. & Guthrie, B. L. Size and distribution of movement fields in the monkey superior colliculus. *Brain Res* **113**, 21-34 (1976).

34 Mante, V., Sussillo, D., Shenoy, K. V. & Newsome, W. T. Context-dependent computation by recurrent dynamics in prefrontal cortex. *Nature* **503**, 78-84 (2013).

35 Rigotti, M. *et al.* The importance of mixed selectivity in complex cognitive tasks. *Nature* **497**, 585-590 (2013).

36 Stokes, M. G. *et al.* Dynamic coding for cognitive control in prefrontal cortex. *Neuron* **78**, 364-375 (2013).

37 Ottes, F. P., Van Gisbergen, J. A. & Eggermont, J. J. Visuomotor fields of the superior colliculus: a quantitative model. *Vision Res* **26**, 857-873 (1986).